Received: 13 July 2022 | Revised: 30 August 2022 | Accepted: 20 September 2022

DOI: 10.1111/cas.15599

Cancer Science WILEY

ORIGINAL ARTICLE

Drug formulation augments the therapeutic response of carboplatin administered through a lymphatic drug delivery system

Radhika Mishra[1] | Ariunbuyan Sukhbaatar[1,2] | Arunkumar Dorai[3] | Shiro Mori[1,2] | Kiyoto Shiga[4,5] | Tetsuya Kodama[1,2]

[1]Laboratory of Biomedical Engineering for Cancer, Graduate School of Biomedical Engineering, Tohoku University, Sendai, Japan

[2]Biomedical Engineering Cancer Research Center, Graduate School of Biomedical Engineering, Tohoku University, Sendai, Japan

[3]Institute of Multidisciplinary Research for Advanced Materials, Tohoku University, Sendai, Japan

[4]Department of Otolaryngology-Head & Neck Surgery, Iwate Medical University, Yahaba, Japan

[5]Head & Neck Cancer center, Iwate Medical University Hospital, Yahaba, Japan

Correspondence
Tetsuya Kodama, Laboratory of Biomedical Engineering for Cancer, Graduate School of Biomedical Engineering, Tohoku University, 4-1 Seiryo, Aoba, Sendai, Miyagi 980-8575, Japan.
Email: kodama@tohoku.ac.jp

Funding information
Japan Society for the Promotion of Science, Grant/Award Number: 20H00655, 20K20161, 21K18319 and 22K18203; Suzuken Memorial Foundation

Abstract

Treatment of metastatic lymph nodes (LNs) is challenging due to their unique architecture and biophysical traits. Systemic chemotherapy fails to impede tumor progression in LNs due to poor drug uptake and retention by LNs, resulting in fatal systemic metastasis. To effectively treat LN metastasis, achieving specific and prolonged retention of chemotherapy drugs in the tumor-draining LNs is essential. The lymphatic drug-delivery system (LDDS) is an ultrasound-guided drug-delivery methodology for administration of drugs to LNs that addresses these requirements. However, early-stage metastatic LNs have an additional set of drug transport barriers, such as elevated intranodal pressure and viscosity, that negatively impact drug diffusion. In the present study, using formulations of elevated osmotic pressure and viscosity relative to saline, we sought to favorably alter the LN's physical environment and study its impact on pharmacokinetics and consequently the therapeutic efficacy of carboplatin delivered using the LDDS. Our study confirmed the capability of a drug formulation with elevated osmotic pressure and viscosity to alter the architecture of LNs, as it caused notable expansion of the lymphatic sinus. Additionally, the study delineated an optimal range of osmotic pressure and viscosity, centered around 1897 kPa and 11.5 mPa·s, above and below which therapeutic efficacy was found to decline markedly. These findings suggest that formulation osmotic pressure and viscosity are parameters that require critical consideration as they can both hinder and promote tumorigenesis. The facile formulation reported here has wide-ranging applicability across cancer spectrums and is thus anticipated to be of great clinical benefit.

KEYWORDS
carboplatin, drug formulation, lymph node metastasis, lymphatic drug-delivery system (LDDS), osmotic pressure, viscosity

Abbreviations: HE, hematoxylin and eosin; i.v., intravenous; ICG, indocyanine green; ICP MS, inductively coupled plasma mass spectroscopy; INP, intranodal pressure; IVIS, in vivo imaging system; LDDS, lymphatic drug-delivery system; LN, lymph node; MLN, metastatic lymph node; MXH10/Mo/lpr, MXH10/Mo-lpr/lpr; MXH51/Mo/lpr, MXH51/Mo-lpr/lpr; PALN, proper axillary lymph node; SiLN, subiliac lymph node.

1 | INTRODUCTION

Despite the great strides made in the early diagnosis and treatment of cancer, worldwide cancer remains a leading cause of death. Prevention and inhibition of fatal systemic metastasis is crucial to curb cancer-associated mortality.[1–5] Tumor-draining lymph nodes (LNs) serve as key facilitators of systemic metastasis as they enable the routing of tumor cells through both the lymphatic and hematogenous network.[6–8] Therefore, therapeutic interventions targeting early-stage metastatic LNs (MLNs) are imperative to limit the systemic spread of cancerous cells which can seed tumors in various remote body organs.

For most solid tumors, complete surgical removal presents itself as the fail-safe approach for tumor eradication, especially at an early stage. However, with respect to MLNs, a consensus regarding the safety and efficacy of lymphadenectomy is lacking.[9–12] Based on the current body of work, there are reasons to believe that lymphadenectomy may result in the activation of dormant tumor cells and be counterproductive. Reports by Sukhbaatar et al.[11] and others have demonstrated links between the dissection of LNs and activation of distant metastasis. Additionally, surgical intervention may not always be feasible. Alternative therapeutic interventions, such as chemotherapy, are routinely used in the clinic for the treatment of MLNs. However, due to the unique architecture and biologics of early-stage MLNs,[13–15] systemic chemotherapy fails to maintain sufficient concentration of drugs in the targeted LN.[16]

The lymphatic drug-delivery system (LDDS) is an ultrasound-guided, intranodal drug-delivery system developed by our group for the effective treatment of MLNs.[17] By achieving drug accumulation specific to tumor-draining LNs and thus localized action in organs crucial to mounting the therapeutic response, the LDDS elicits a strong therapeutic response while minimizing unwarranted effects stemming from systemic exposure to highly toxic drugs. Mainstay chemotherapeutic agents such as cisplatin and fluorouracil (5-FU), administered through the LDDS in a murine model of LN metastasis, have shown superior tumor inhibition compared to their systemic administration in the same model.[16,18–20] While the LDDS addresses certain limitations of systemic chemotherapy, and exerts a stronger antitumor effect, further fine-tuning is mandated for potentiation of the beneficial antitumor effects.

Emerging data points to the existence of bidirectional links between the physical traits and biological hallmarks of cancer. Drug viscosity is known to affect diffusion and thereby permeation of injected fluids into solid tumors.[21,22] Elevated intranodal pressure (INP) can be utilized as a diagnostic tool for early-stage MLNs. A correlation between INP and therapeutic response has also been established by our group.[23] Additionally, previous studies have attributed pin prick leak, that is, drug leakage from pin prick due to uniformly elevated interstitial fluid pressure in solid tumors, to explain insufficient drug accumulation in the target tissue.[21] It is likely that the same effect is exerted in the case of localized administration of chemotherapeutic agents to MLNs, that is, high intranodal pressure results in the leakage of injected drug solution out of the needle puncture, resulting in a pin prick leak. Such biophysical anomalies, including elevated INP and viscosity, etc. of the tumor microenvironment, impact drug convection[24–27] and dynamically interact with the biochemical microenvironment to facilitate the metastatic transition of tumor cells.[28–32] In the same vein, our group hypothesized that modification of tumor biomechanics or the biophysical environment may affect drug convection, thereby maximizing the potency of drug administered through the LDDS. Taking these points into consideration, our group sought to uncover whether drug solvent physicochemical parameters, for example osmotic pressure and viscosity, could positively influence drug permeation and thereby the therapeutic response of an administered drug. Previous studies undertaken by our group, using cisplatin and docetaxel, have touched on and verified the impact of solvent osmotic pressure and viscosity on anticancer effect elicited by chemotherapeutic agents in the context of MLNs.[19,20] However, while these studies have highlighted the importance of these parameters, osmotic pressure and viscosity have not been independently investigated. This study was designed to evaluate the individual contributions of elevated osmotic pressure and viscosity on the therapeutic response and to establish an optimized window of solvent osmotic pressure and viscosity for treatment of MLNs using the LDDS. While technical constraints did not permit the study of solutions with increasing viscosity and constant osmotic pressure, solutions with the same osmotic pressure but different viscosity were investigated. Solutions spanning 588 kPa–2785 kPa osmotic pressure and 0.9 mPa·s–54.6 mPa·s viscosity were tested for therapeutic efficacy using the LDDS.

Based on our findings, herein we report a facile drug formulation that addresses the shortcomings of systemic therapy for the treatment of MLNs, thereby markedly increasing drug efficacy.

2 | MATERIALS AND METHODS

2.1 | Mice

MXH10/Mo-lpr/lpr (MXH10/Mo/lpr) and MXH51/Mo-lpr/lpr (MXH51/Mo/lpr) mice were utilized for this study.[33] These mice permit reliable interrogation of LN pathogenesis.

2.2 | Tumor-bearing LN mouse model

To establish a murine model-bearing tumor in the LN, FM3A-Luc cells were inoculated into the subiliac lymph node (SiLN) of MXH10/Mo/lpr mice. The day of inoculation was defined as day 0.

2.3 | Drug formulation

Eight solutions, with different key constituent and physicochemical parameters (Table 1 and Figure S1), were prepared. Solutions consisted primarily of either glucose (Otsuka Pharmaceutical) or

TABLE 1 Drug formulation details

Formulation main component	Formulation properties		Formulation name		Administration strategy	Injection rate	Experimental group name	
	Osmotic pressure (kPa)	Viscosity (mPa·s)	CBDCA–	CBDCA+			CBDCA–	CBDCA+
Glucose	588	0.9	G 0	CG 0	i.v.	Bolus	G 0 [I]	CG 0 [I]
Glucose	588	0.9	G II	CG 0	LDDS	10 μL/min	G II [L]	CG 0 [L]
Glucose	1177	0.9		CG I	LDDS			CG I [L]
Glucose	1897	0.9		CG II	LDDS			CG II [L]
Glucose	2785	0.9		CG III	LDDS			CG III [L]
Polysorbate80	1177	6	P II	CP I	LDDS		P II [L] (Placebo)	CP I [L]
Polysorbate80	1897	11.5		CP II	LDDS			CP II [L]
Polysorbate80	2785	54.6		CP III	LDDS			CP III [L]

Note: The presence of carboplatin (CBDCA) in the solution is denoted by the letter 'C', 'P/G' denote polysorbate80 or glucose as the primary component of the formulation, the Roman numerals (0/I/II/III) following the letter indicate the physicochemical parameters of the resultant formulation. 'I/L', for intravenous (i.v.) or lymphatic drug-delivery system (LDDS), respectively, indicates the route of administration.

polysorbate80 (NOF). The osmotic pressure and viscosity of solutions tested ranged from 588 to 2785 kPa and 0.9 mPa·s to 54.6 mPa·s, respectively, and were calculated from theory and experimentally verified as previously described.[19,20]

2.4 | Biodistribution of carboplatin administered by different routes

CG 0 was administered intravenously and CG I was administered through the LDDS at 10 μl/min to MXH10/Mo/lpr mice devoid of tumor, to quantify accumulation in the subiliac lymph node (SiLN), proper axillary lymph node (PALN), kidney, liver, and lung immediately post-drug administration, on day 0^T, and at the pre-determined experimental endpoint, day 9^T. On day 0^T or on day 9^T, mice were euthanized and SiLN, PALN, kidney, liver, and lung excised. Harvested organs were then processed for ^{195}Pt quantification by inductively coupled plasma mass spectroscopy (ICP MS).

2.5 | In vivo pharmacokinetic characterization of drug formulations with varying physicochemical parameters

To evaluate whether changing the physicochemical parameters of the formulation had any effect on its pharmacokinetics, formulation G 0 was administered intravenously (bolus), or formulations G II or P II were administered via LDDS (10 μl/min) to tumor-free MXH51/Mo/lpr mice. Biofluorescent imaging was performed using an in vivo imaging system, in vivo imaging system (IVIS; PerkinElmer), before administration and at various time points after administration of formulation to monitor the indocyanine green (ICG) fluorescence. The ICG concentration at various time points was determined using[34]:

$$[\mathrm{ICG}] = \frac{[\mathrm{FI}(t) - \mathrm{FI}(0\mathrm{BT})]}{[\mathrm{FI}(T\mathrm{max}) - \mathrm{FI}(0\mathrm{BT})]} \times \frac{[\text{ICG injected concentration X ICG injected volume}]}{\text{lymph volume} + \text{ICG injected volume}}$$

where FI(t) is the fluorescence intensity captured over the SiLN at time t, FI(0_{BT}) is the fluorescence intensity captured over the SiLN prior to formulation administration, and FI(T_{max}) is the fluorescence intensity captured over the SiLN when maximum fluorescence intensity was detected over the SiLN. The ICG injected concentration was 0.1 mg/ml, the ICG injected volume was 0.2 ml, and the lymph volume was 46.5 μl.

FI(t), FI(0_{BT}), and FI(T_{max}) were experimentally determined. Lymph volume in the SiLN was determined experimentally by determining the volume of contrast agent retained in the SiLN immediately post-administration of 200 μl of barium contrast agent.[35]

The pharmacokinetic parameters were determined using a non-compartmental model.

Additionally, to confirm these findings in a tumor-bearing murine model, MXH10/Mo/lpr mice inoculated with FM3A-Luc cells were administered formulations of varying osmotic pressure and viscosity on day 7 as described.

CG 0 was administered intravenously (bolus) or through the LDDS (10 μl/min), and P II, CG I, CG II, CG III, CP I, CP II, and CP III were administered through the LDDS (10 μl/min).

In vivo biofluorescent imaging was performed on day 7 before and after treatment, and on days 10, 13, and 16 using IVIS to quantify the fluorescent intensity over the SiLN and PALN to monitor drug formulation retention. For graphical representation, in vivo fluorescence data were normalized to its value obtained prior to treatment on day 7.

On day 16, mice were euthanized and ex vivo biofluorescent imaging of the SiLN, PALN, liver, and lung were performed using IVIS to quantify the accumulation of the formulation in these organs. For ex vivo graphical representation, raw biofluorescent intensity, as measured by IVIS, was used as is.

2.6 | Effect of drug formulation on the therapeutic response

Drug was administered to tumor-bearing LN mice as described in the previous section. In vivo bioluminescent imaging was performed on days 7, 10, 13, and 16 using IVIS to estimate the tumor growth. Luciferase activity recorded was normalized to its day 7 value for graphical representation.

SiLN and PALN volumes were measured on days 0, 7, 10, 13, and 16 using a high-frequency ultrasound device, VEVO770 (FUJIFILM VisualSonics). LN volumes were normalized to their day 0 value for subsequent analysis. Body weight was recorded, and mice were monitored for any chemotherapy-induced toxicity.

2.7 | Histological analysis

Hematoxylin and eosin staining of SiLN and PALN harvested on day 16 was performed to confirm tumor growth/inhibition.

2.8 | Statistical analysis

Graphpad Prism 8.4.3 (GraphPad Software) and Microsoft Excel were used to perform all statistical analyses.

3 | RESULTS

3.1 | Biodistribution and retention of carboplatin administered via different drug delivery routes

First, the retention of carboplatin solution administered by different routes was characterized. The Pt content in various organs after a single intravenous (i.v.) injection at 588 kPa, 0.9 mPa·s, or a single intranodal injection of CDDP solution at 1897 kPa, 0.9 mPa·s to tumor-free mice was determined on day 0^T and day 9^T using ICP MS

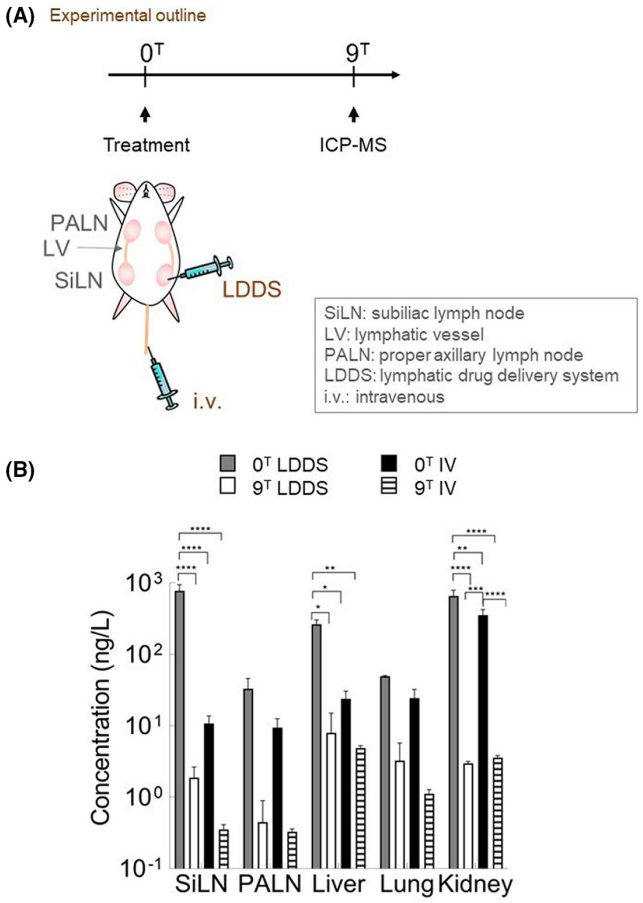

FIGURE 1 Quantification of carboplatin (CBDCA) retained in various organs after administration through different drug-delivery routes on days 0^T and 9^T. (A) Experiment outline. Carboplatin formulation CG 0 was delivered intravenously and using the lymphatic drug-delivery system (LDDS) on day 0^T. Subsequently, Pt concentration was evaluated in the SiLN, PALN, liver, lung, and kidney on day 0^T or day 9^T. (B) Platinum quantification in various organs as measured by inductively coupled plasma mass spectroscopy. Delivery of formulation using LDDS resulted in specific delivery to the SiLN, whereas intravenous (i.v.) delivery produced nonspecific delivery to highly perfused organs. 0^T LDDS, $n = 3$; 9^T LDDS, $n = 3$; 0^T i.v., $n = 3$; 9^T i.v., $n = 4$. PALN, proper axillary lymph node; SiLN, subiliac lymph node.

(Figure 1A). Acquired data were used to study the biodistribution of carboplatin in the SiLN, PALN, liver, lung, and kidney as a function of time (day 0^T and 9^T). Table 2 shows the percentage of carboplatin delivered to various organs considering solely the organs examined in the present study. Administration through the LDDS resulted in maximal delivery to the intended site, the SiLN, with comparable amount of drug retained in the kidney. Contrary to delivery through the LDDS, i.v. delivery resulted in maximal accumulation of the drug in the kidney on day 0^T (32 times higher than in the SiLN). In this case, on day 0^T, the SiLN and PALN were found to receive comparable amounts of carboplatin.

Comparison between the drug administration strategies revealed that on day 0^T greater Pt accumulation to SiLN, PALN, liver,

TABLE 2 Biodistribution and retention of carboplatin delivered to the SiLN through the LDDS or intravenously

	Biodistribution (0^T) (% of total)		Retention ($0^T/9^T \times 100\%$)		LDDS/i.v.	
	LDDS	i.v.	LDDS	i.v.	0^T	9^T
SiLN	43.65	2.56	0.24	3.25	71.77	5.36
PALN	1.86	2.23	1.35	3.49	3.50	1.36
Liver	14.80	5.62	3.04	20.50	11.06	1.64
Lung	2.77	5.76	6.60	4.56	2.03	2.93
Kidney	36.93	83.84	0.45	1.01	1.85	0.83

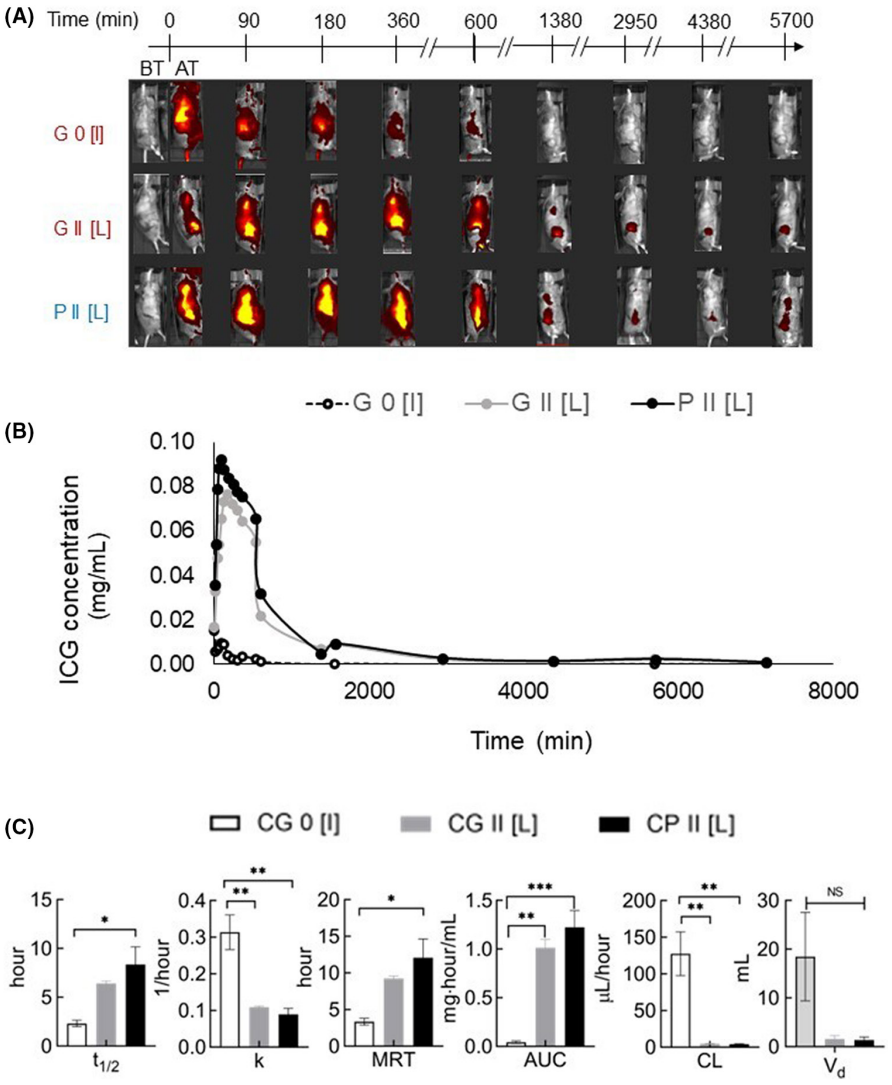

FIGURE 2 Pharmacokinetic profiling of formulations with varying osmotic pressures and viscosities administered through the lymphatic drug-delivery system (LDDS) or i.v. (A) Representative biofluorescent images at selected time points. ICG accumulation in the subiliac lymph node and proper axillary lymph node was monitored in tumor-free MXH51/Mo/lpr mice post-administration of formulation G 0 i.v. or G II through the LDDS or P II through the LDDS. (B) ICG concentration–time curve. (C) Pharmacokinetic characterization of formulations G 0, G II, and P II administered as described above. G 0 [I], $n = 3$; G II [L], $n = 3$; P II [L], $n = 3$. AUC, area under the concentration–time curve; CL, clearance; C_{max}, maximum concentration of ICG detected in the lymph node; ICG, indocyanine green; k, fractional rate of elimination; MRT, mean residence time; $t_{1/2}$, half-life; T_{max}, time at which C_{max} was achieved; V_d, volume of distribution.

lung, and kidney was achieved by administration through the LDDS (Figure 1B and Table 2).

By day 9^T, only a miniscule amount of drug was retained in the organs after the use of both drug-delivery strategies. The percentage retention in all organs except the lung was higher after i.v. delivery of the drug (Table 2). However, even on day 9^T, the amounts of drug retained in the SiLN, PALN, liver, and lung were higher after administration of drug through the LDDS, but the amount of drug retained in the kidney on day 9^T after i.v. administration was found to be slightly higher compared to administration of drug through the LDDS (Figure 1B).

Thus, LDDS was found to be a superior drug administration strategy in comparison to i.v. delivery for the treatment of MLNs.

3.2 | In vivo pharmacokinetics and biodistribution of drug formulations with varying physicochemical parameters

Having verified a highly specific biodistribution of LDDS in comparison to i.v. drug delivery, the next set of experiments focused on discerning the relevance of solvent osmotic pressure and viscosity

TABLE 3 Pharmacokinetic parameters of drug formulations having different osmotic pressures and viscosities after administration in tumor-bearing MXH10/Mo/lpr mice intravenously or via lymphatic drug-delivery system

Group	C_{max} (mg/ml)	T_{max} (h)	$t_{1/2}$ (h)	*k* (1/h)	MRT (h)	ICG dose (μg)	AUC (mg×h/ml)	CL (SiLN) (μl/h)	V_d (apparent) (ml)
G 0 [I]	0.009 ± 0.001	1.5	2.31 ± 0.33	0.314 ± 0.047	3.33 ± 0.48	4.65	0.04 ± 0.01	127.52 ± 29.97	18.46 ± 9.07
G II [L]	0.077 ± 0.003	3	6.41 ± 0.23	0.108 ± 0.004	9.25 ± 0.33		1.01 ± 0.09	4.67 ± 0.44	1.53 ± 0.74
P II [L]	0.092 ± 0.017	1.5	8.37 ± 1.78	0.090 ± 0.016	12.08 ± 2.57		1.22 ± 0.17	3.96 ± 0.57	1.34 ± 0.66

Abbreviations: AUC, area under the concentration-time curve; CL, clearance; C_{max}, maximum concentration of ICG detected in the lymph node; ICG, indocyanine green; *k*, fractional rate of elimination; MRT, mean residence time; SiLN, subiliac lymph node; $t_{1/2}$, half-life; T_{max}, time at which C_{max} was achieved; V_d, volume of distribution.

for drug delivery through the LDDS. First, in a tumor-free mouse model, a pharmacokinetic characterization of the drug formulations at various osmotic pressures and viscosities delivered either intravenously or using the LDDS was performed. Biofluorescent images of selected time points are shown in Figure 2A. After i.v. delivery of G 0, immediately post-administration, the biofluorescent intensity was found to be centered around highly perfused organs, including the liver and lung. However, delivery of G II and P II through the LDDS was found to result in higher fluorescent signals concentrated around the SiLN and PALN, indicative of highly specific delivery to these sites. Of note, the fluorescent signal over the SiLN was found to be higher in group P II [L]. Within 24 h, the fluorescent intensity in group G 0 [I] was shown to drop below the minimum threshold. However, strong fluorescent intensity could be detected in G II [L] and P II [L] at this time point. Additionally, fluorescent intensity, and therefore the concentration of ICG accumulated in the SiLN in group P II [L], was found to be consistently higher than that of G II [L] and G 0 [I], indicative of its superior pharmacokinetics. Table 3 summarizes the calculated pharmacokinetic parameters for G 0 [I], G II [L], and P II [L]. The $t_{1/2}$, MRT and AUC of P II [L] were the highest, while *k*, CL, and V_d were found to be the least for group P II [L], indicative of the exceptional pharmacokinetics of formulation P II delivered through the LDDS (Figure 2B,C).

In addition, to confirm these findings in a murine MLN model, drug formulations of varying osmotic pressures and viscosities (Table 1 and Figure S1) containing ICG were administered to MXH10/Mo/lpr mice with tumors in the SiLN and imaged using IVIS to profile the retention of the formulation in the SiLN and PALN (Figure 3A). Consistent with the findings of the pharmacokinetic study in the tumor-free murine model, i.v. administration resulted in nonspecific delivery throughout the body whereas drug delivery through the LDDS with all formulations investigated showed higher fluorescent signals concentrated around the SiLN and PALN. Among formulations delivered through the LDDS, significantly higher delivery to the SiLN and PALN was achieved in the CP I [L], CP II [L], and CP III [L] groups compared to the CG 0 [L], CG I [L], CG II [L], and CG III [L] groups. On day 7, immediately after drug administration, no apparent differences in normalized fluorescent intensity in the SiLN were detected among drug formulations comprising glucose at different osmotic pressures (1176–2785 kPa, 0.9 mPa·s) or drug formulations comprising polysorbate80 at different osmotic pressures (1176–2785 kPa) and viscosities (6–54.6 mPa·s); differential retention tendencies were apparent on subsequent experimental days.

Overall, a progressive decline in biofluorescent intensity with time was observed. However, the clearance rate varied between the groups. Coherent with ICP MS and pharmacokinetic profiling in tumor-free model results, clearance of drug formulations delivered intravenously was remarkably fast (Figure 3B). In the i.v. drug-delivery group (CG 0 [I]), the formulation was found to clear completely 3 days after administration (day 10) as evidenced by the return of fluorescence levels in the SiLN and PALN below the set threshold. In contrast, in the SiLN, retention up to day 16 was found for all LDDS groups. Formulations with polysorbate80 as a

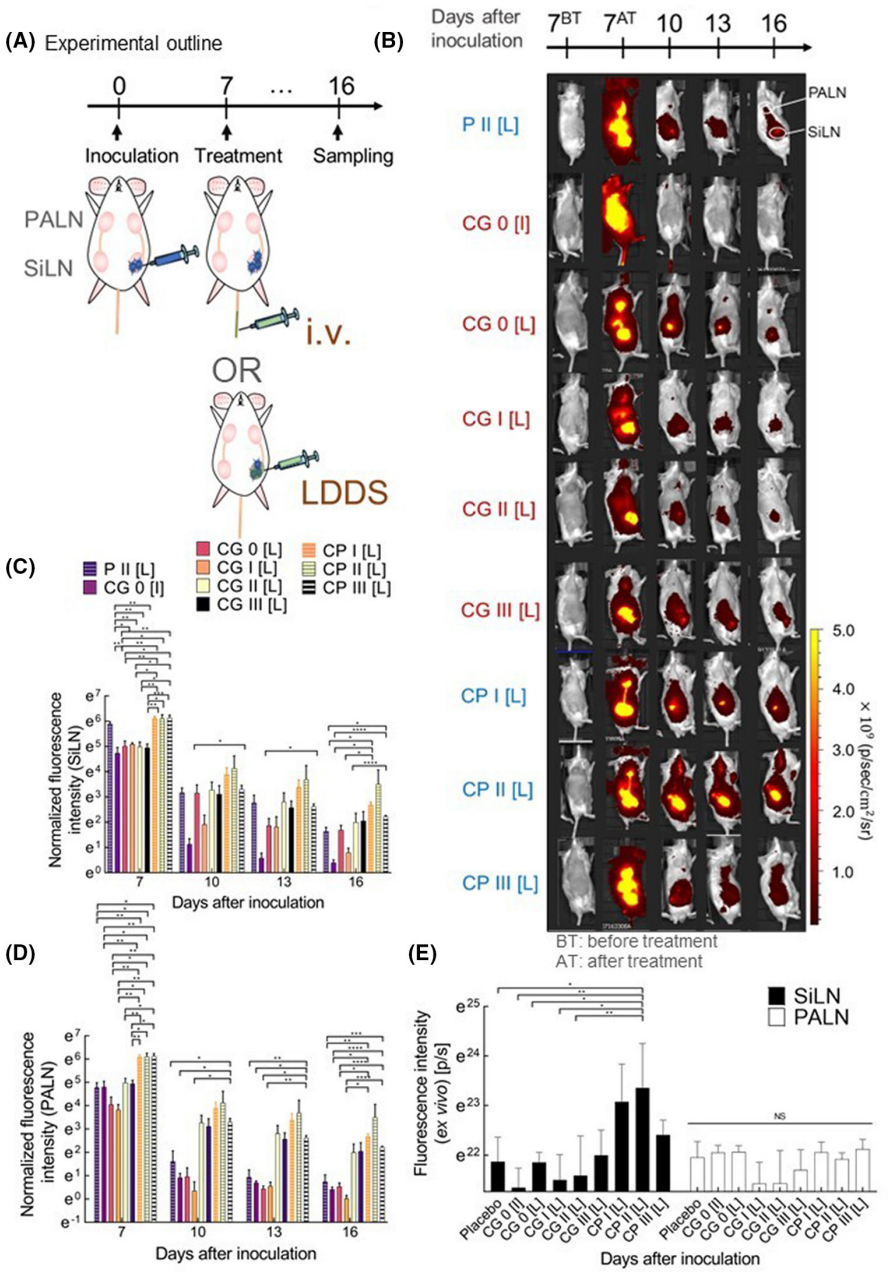

FIGURE 3 Retention of modified drug formulations in tumor-bearing and downstream lymph nodes. (A) Experiment outline. Drug accumulation at the target site was evaluated by biofluorescent imaging of indocyanine green solution that was co-administered with the formulation in a tumor-bearing murine model. Formulations were administered to the different groups as indicated in Table 1, 7 days post-tumor inoculation. Drug accumulation was measured on days 7, 10, 13, and 16 post-tumor inoculation. (B) Representative in vivo biofluorescent imaging. (C) Quantitative analysis of in vivo biofluorescent intensity over the subiliac lymph node (SiLN). (D) Quantitative analysis of in vivo biofluorescent intensity over the proper axillary lymph node (PALN). Prolonged retention at targeted sites, the SiLN and PALN, was observed in the CP II [L] group, indicative of the superior pharmacokinetic profile of the CP II formulation administered using the lymphatic drug-delivery system. (E) Quantitative analysis of ex vivo biofluorescent intensity of the SiLN and PALN. P II [L], $n = 7$; G 0 [I], $n = 7$; G 0 [L], $n = 7$; G I [L], $n = 9$; G II [L], $n = 8$; G III [L], $n = 6$; P I [L], $n = 5$; P II [L], $n = 8$; P III [L], $n = 5$. i.v., intravenous.

constituent were found to show markedly stronger fluorescence signals in both the SiLN and PALN at all time points investigated (days 10, 13, and 16) (Figure 3B–D). Fluorescent intensity, and thereby formulation retention, in the SiLN and PALN on day 16 was found to be particularly pronounced in the CP II [L] group (1897 kPa, 11.5 mPa·s; LDDS). In this group, around 33.33% of the formulation delivered to the SiLN and 3.8% of the formulation delivered to the PALN on day 7 was found to persist in the SiLN and PALN, respectively, on day 16. Drug formulations retained in the SiLN and PALN in this group were found to be consistently the highest (day 10 onwards) (Figure 3C,D).

These results indicate the superior in vivo pharmacokinetics demonstrated by P II formulation administered with or without the drug carboplatin, delivered through the LDDS (P II [L] or CP II [L]).

3.3 | Antitumor efficacy of carboplatin formulations with varying physicochemical parameters

To determine whether osmotic pressure and viscosity had any impact on therapeutic response, drug formulations were administered to MXH10/Mo/lpr mice bearing tumor in the SiLN and tumor progression was regularly monitored (Figure 4A). On day 10, tumor progression rates were found to differ markedly between groups (Figure 4B,C). Longitudinal analysis of tumor progression revealed tumor growth at a steady rate in the control and placebo groups. In comparison to the control group, all groups except for placebo (PL II) showed significantly decelerated tumor progression until day 16. However, carboplatin formulation of 588 kPa osmotic pressure and 0.9 mPa·s viscosity delivered intravenously

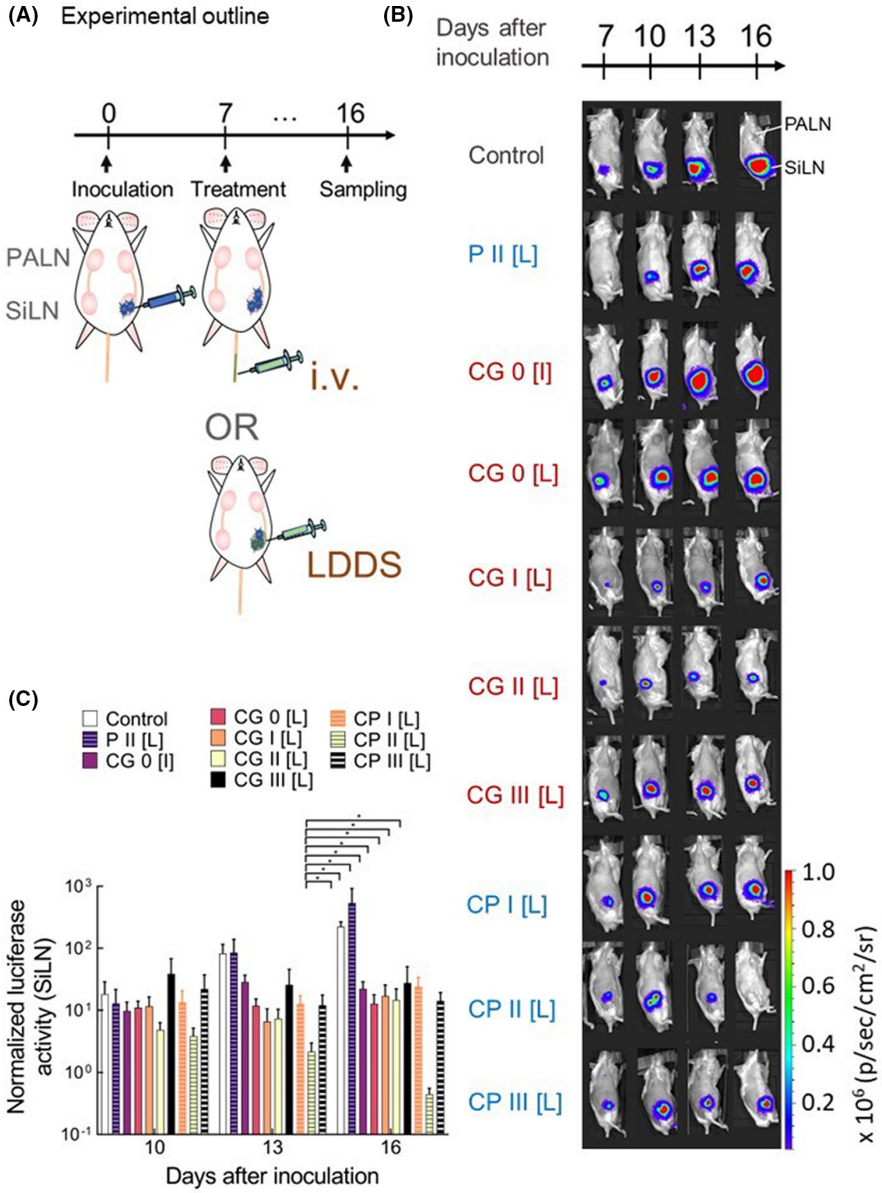

FIGURE 4 Tumor inhibition after administration of a modified drug formulation. (A) Experiment outline. Tumor progression post-drug formulation administration was monitored every 3 days until the pre-determined endpoint of each experiment. Formulations were administered to the different groups as indicated in Table 1, day 7 post-tumor inoculation. (B) Representative in vivo bioluminescent images. (C) Quantitative analysis of in vivo bioluminescent imaging of the SiLN. A remarkable reduction in the tumor burden was observed in the SiLN of the CP II [L] group. Control, $n = 9$; P II [L], $n = 6$; G 0 [I], $n = 7$; G 0 [L], $n = 7$; G I [L], $n = 8$; G II [L], $n = 7$; G III [L], $n = 6$; P I [L], $n = 5$; P II [L], $n = 6$; P III [L], $n = 5$. i.v., intravenous; LDDS, lymphatic drug-delivery system; PALN, proper axillary lymph node; SiLN, subiliac lymph node.

was found to be inferior in terms of antineoplastic activity in comparison to carboplatin delivered through the LDDS admixed into a formulation of the same osmotic pressure and viscosity; delivery of the CG 0 through LDDS resulted in an additional 50% reduction in tumor burden compared to its administration intravenously (Figure 4B,C).

Among the groups in which the drug formulation comprising primarily glucose was administered through the LDDS, maximum tumor inhibition was observed in the CG II [L].

Among the groups in which the drug formulation comprising primarily polysorbate80 was delivered through the LDDS, tumor inhibition was the strongest for CP II [L] (Figures 4B,C and S2A). In addition, this group was also found to exhibit the strongest tumor inhibition overall, with a 55.2% reduction in tumor burden relative to day 7 at the pre-determined endpoint. Additionally, unlike other groups, a marked and steady decline in luciferase activity was observed from day 10 onwards in this group (Figure 4C).

Findings from histological analyses were found to corroborate the conclusion derived from bioluminescent imaging (Figure 5). Uninhibited tumor proliferation was observed in the control and P II [L] groups, with intra- and extranodular invasion of tumor cells. Intravenous delivery of the CG 0 formulation was ineffective for the treatment of SiLN, with tumor cells found to be populating most of the LN. Tumor cell infiltration in the SiLN of CGII [L] group was moderate, indicative of mild tumor inhibition. Remarkably, no tumor cells were found in most areas of the hematoxylin and eosin-stained sections of the SiLN that were treated with the CP II formulation intranodaly, indicative of successful suppression of tumor growth. Additionally, a dilation of the lymphatic sinus was observed. In some sections, chemotherapy-induced fibrosis was noted (Figure 5). In one out of eight slides, the parenchyma was found to be replaced by necrotic tissue.

Consistent with the lack of tumor inhibition, SiLN volumes were found to be increased in the control, placebo, and i.v. drug delivery

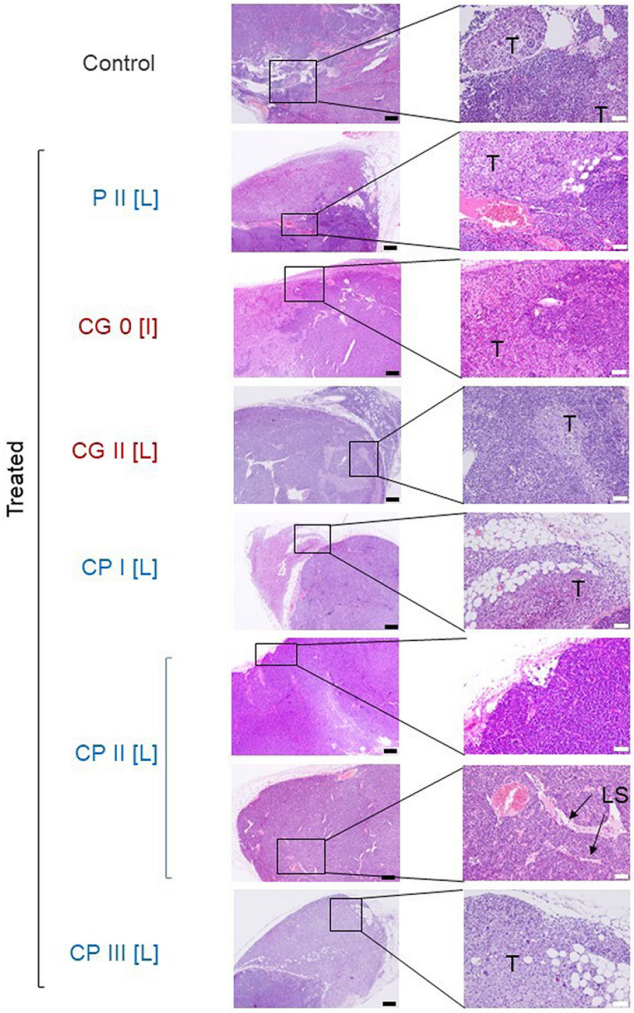

FIGURE 5 Histological evaluation of hematoxylin and eosin (HE)-stained sections of subiliac lymph node (SiLN) after administration of a modified drug formulation. HE-stained sections of the SiLN in the control and treated groups of tumor-bearing MXH10/Mo/lpr mice, 16 days post-tumor cell inoculation. A formulation, with or without carboplatin, at the indicated osmotic pressure and viscosity was administered either intravenously or into the SiLN using the lymphatic drug-delivery system, as indicated in the treatment group on day 7. High magnification images of the highlighted regions are presented to the right. In the control, P II [L] and CG 0 [I] groups, strong uninhibited tumor proliferation with intra- and extranodular invasion was observed. Tumor cell infiltration in the SiLN of the CG II [L] group was moderate, indicative of mild tumor inhibition. Tumor cells were absent from the parenchyma of most SiLN of the CP II [L] group, indicative of successful suppression of tumor growth. In some cases, the parenchyma was found to be replaced in part by necrotic tissue. Additionally, expansion of the lymphatic sinus was observed in the SiLN of this group. Control, $n = 5$; P II [L], $n = 5$; G 0 [I], $n = 6$; G 0 [L], $n = 7$; G II [L], $n = 4$; P I [L], $n = 5$; P II [L], $n = 5$; P III [L], $n = 5$. LS, lymphatic sinus; T, tumor cell; Scale bars: 200 μm (black) and 50 μm (white).

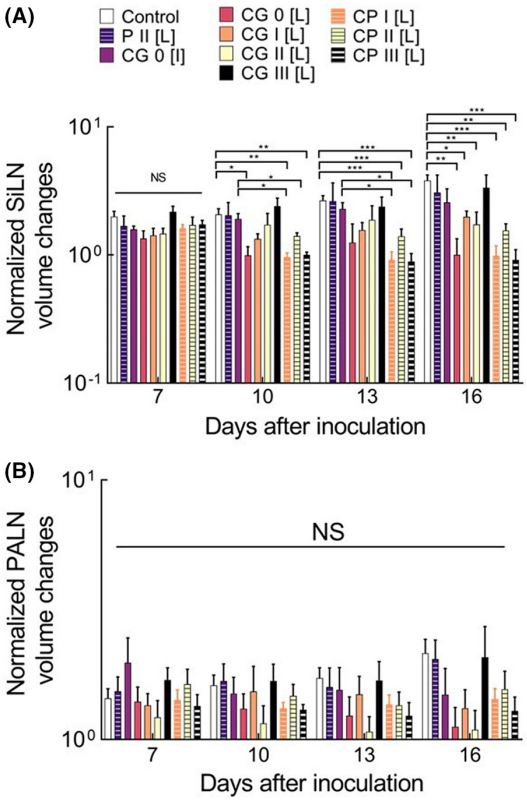

FIGURE 6 Lymph node volume changes after administration of modified drug formulations in a tumor-bearing lymph node (LN) mouse model. SiLN and PALN volumes were measured on days 0, 7, 10, 13, and 16 in tumor inoculated MXH10/Mo/lpr mice. LN volumes on each experimental day were normalized with respect to their day 0 values to permit monitoring of the rate of increment of LN volumes. (A) Normalized SiLN volume. (B) Normalized PALN volume. Control, $n = 9$; P II [L], $n = 7$; G 0 [I], $n = 7$; G 0 [L], $n = 7$; G I [L], $n = 9$; G II [L], $n = 8$; G III [L], $n = 6$; P I [L], $n = 5$; P II [L], $n = 7$; P III [L], $n = 5$. NS, not significant; PALN, proper axillary lymph node; SiLN, subiliac lymph node.

groups. From days 7 to 10, the normalized SiLN volumes of the CP I [L]–III [L] group were found to decrease and subsequently, i.e., day 10 onwards, stabilized. Of great interest, in the CP I [L] and CP III [L] groups, although tumor suppression was not on a par with that observed after CP II [L], the normalized SiLN volume was found to be less than for CP II [L] on days 10, 13, and 16 (Figure 6A). Normalized PALN volumes on day 16 for CP I [L], CP II [L], and CP III [L] groups were also found to follow a similar trend (Figure 6B). However, differences in normalized PALN volumes, if any, were found to be insignificant. Notably, such counterintuitive results were not observed in the CG I [L], CG II [L], and CG III [L] groups (Figure 6A,B). In addition, no remarkable decline in body weight (Figure 7) or treatment-associated morbidity was observed in any of the groups, indicating that all treatments were well tolerated.

4 | DISCUSSION

Carboplatin is a mainstay chemotherapy approved and widely used for the treatment of head and neck, ovarian, and lung cancers, among others. While i.v. administration of carboplatin dissolved in saline

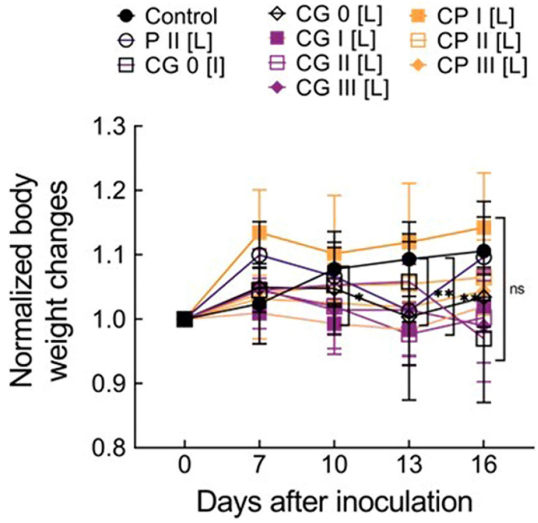

FIGURE 7 Normalized body weight changes. Body weight was measured on days 0, 7, 10, 13, and 16 in MXH10/Mo/lpr mice inoculated with tumor cells and treated with formulations having different osmotic pressures and viscosities. Body weight was normalized with respect to its value on day 0. Control, $n = 9$; P II [L], $n = 7$; G 0 [I], $n = 7$; G 0 [L], $n = 7$; G I [L], $n = 9$; G II [L], $n = 8$; G III [L], $n = 6$; P I [L], $n = 5$; P II [L], $n = 7$; P III [L], $n = 5$.

has produced encouraging results, huge scope for improvement remains.[36] Innovations in drug formulation and delivery strategy are crucial for potentiating the therapeutic effect of chemotherapeutic drugs.[22] Herein, we studied the impact of the drug-delivery route and the osmotic pressure and viscosity of its formulation on biodistribution and in vivo pharmacokinetics, and consequently on the therapeutic efficacy of carboplatin administered through the LDDS for the treatment of MLNs.

Taking normal tissue tolerance into account is critical in limiting chemotherapy-associated morbidity. We found that while i.v. administration resulted in maximal delivery to highly perfused organs such as the kidney, lung, and liver, intranodal delivery produced maximal delivery to the targeted organ, the SiLN. As per our findings, through i.v. administration, achieving accumulation of drug in the SiLN equivalent to that accumulated through LDDS, to elicit comparable therapeutic responses would require about 72 times the drug concentration administered through the LDDS. This is in agreement with previous findings, which established the requirement of drastically reduced concentrations of drug when administered through the LDDS as opposed to intravenously for achieving a similar therapeutic response.[16,18–20] It is important to note, however, that delivery at increased concentrations intravenously would cause significantly higher levels of nonspecific accumulation of drug. This finding, paired with a higher percentage retention in most organs after i.v. delivery, would imply accumulation of potentially detrimental levels of carboplatin in unintended organs for prolonged periods, resulting in potentially fatal systemic toxicity. Intravenous administration thus necessitates a trade-off between the therapeutic response and toxicity for the treatment of MLNs. Such a trade-off is not mandated in the case of drug delivery through the LDDS. Furthermore, drug delivery through the LDDS was also found to achieve about 3.5 times higher concentration in the PALN compared to i.v. administration, indicating the potential of the LDDS to treat downstream MLN and reinforcing previous findings.[19] These results, in concert with previous reports, show that LDDS will be a suitable therapeutic intervention to greatly enhance the clinical treatment of MLNs.

Biomechanical cues stemming from physical disruptions in the tumor microenvironment are known to play a prominent role in tumorigenesis. These anomalous physical traits not only affect drug transport and tissue penetration,[22] but also relay signals to a huge array of mechanosensitive signaling pathways.[29–31] Therefore, it is expected that therapeutic interventions favorably modifying the tumor biomechanical environment promote tumor eradication. Our group thus sought to devise simple strategies to alter tumor biomechanics, thereby promoting favorable drug convection and/or triggering a tumor-suppressive signaling cascade. We hypothesized that solvents having elevated osmotic pressure and viscosity administered intranodaly could transiently disrupt the LN architecture and thus its physical microenvironment, positively affecting the therapeutic efficacy of an intranodaly administered drug.

Consistent with our hypothesis, dilation of the lymphatic sinus for maintenance of osmotic homeostasis in the LN after intranodal delivery of carboplatin formulation of elevated osmotic pressure and viscosity was reported in the present study. Notably, formulations with different osmotic pressures and viscosities were found to show distinct in vivo pharmacokinetic profiles. Formulations with or without carboplatin at an osmotic pressure and viscosity of 1897 kPa and 11.5 mPa·s, respectively, were found to display the most favorable pharmacokinetic parameters.

Additionally, formulation of the same osmotic pressure and viscosity (1897 kPa and 11.5 mPa·s), with carboplatin was reported to elicit the strongest antitumor effect. This remarkable tumor suppression can be attributed to the exceptionally favorable in vivo pharmacokinetics displayed.

Previously, using cisplatin we demonstrated that a formulation of high osmotic pressure and viscosity (1897 kPa, 11.5 mPa·s) delivered through an upstream tumor-free lymph node (SiLN) could substantially decelerate tumor progression in the downstream tumor-bearing LN (PALN) as opposed to cisplatin admixed with saline delivered intravenously. It is important to note that the two studies differed in the following respects: in the present study, the SiLN is the tumor-bearing LN, and it is also the site of administration of a drug formulation, while in the previous study, PALN, the LN downstream of SiLN, was the tumor-bearing LN and SiLN was the LN to which drug was administered. Our biodistribution study confirmed that tumor-localized delivery minimized systemic leakage and enabled maximal drug accumulation in the enestic site, the SiLN. Notably, accumulation immediately after administration to the enestic LN, the SiLN, was about 23 times higher than in the downstream LN, the PALN. Naturally therefore, the magnitude of deceleration observed in the present study was considerably higher than that reported by Fukumura et al.,[19] resulting in fact in a dramatic reduction in tumor mass. A striking 55.2% reduction in

tumor burden in comparison to the date of initiation of treatment was observed at the pre-determined experimental end point after administration of the carboplatin formulation CP II (1897 kPa, 11.5 mPa·s). For all osmotic pressure and viscosity ranges investigated, therapeutic efficacy was found to be considerably enhanced when drug delivery was intratumoral. These findings highlight the importance of the development of targeted drug-delivery strategies to achieve highly specific drug accumulation. Importantly, despite consideration of additional formulations in the present study, the optimal physicochemical parameters were not found to differ. Thus, it follows that optimized range of drug physicochemical parameters for delivery through the LDDS are universal and is around 1897 kPa and 11.5 mPa·s (Figure S2A,B).

While osmotic pressure and viscosity are independent parameters, it appears that they act synergistically as increasing osmotic pressure alone, while maintaining viscosity, does not provide an additional significant therapeutic advantage (Figure S2A,B). However, in both cases, therapeutic efficacy as a function of osmotic pressure was found to saturate at 1897 kPa. Increasing the osmotic pressure of the formulation in concert with viscosity drastically improved the therapeutic response, as evidenced by the remarkably low normalized in vivo luciferase activity on day 16 after administration of the 1897 and 2785 kPa formulation. Pharmacokinetic profiling of the 1897 kPa and 0.9 or 11.5 mPa·s formulations confirmed that this is likely due to sustained release and prolonged retention due to the increased viscosity of the formulation. This hypothesis of a greater MRT and lower clearance was observed for the 1897 kPa and 11.5 mPa·s formulation as opposed to the formulation having the same osmotic pressure but 0.9 mPa·s viscosity. However, as previously reported, administration of a formulation with an osmotic pressure and viscosity greater than 2000 kPa and 12 mPa·s caused mild injection site adverse events. Likewise, we also observed an aberrant decline in the SiLN volume after administration of carboplatin solution containing polysorbate80. This is likely a consequence of treatment-induced destruction of lymphocytes.[19] However, this phenomenon was restricted to the SiLN as an aberrant decline in LN volume was not observed in the PALN.

In conclusion, our results demonstrated that a drug formulation of 1897 kPa osmotic pressure and 11.5 mPa·s viscosity, administered through the LDDS, exhibited superior pharmacokinetics and rendered the LN environment amenable to the actions of a chemotherapeutic agent. An additional advantage of the simple modification in formulation proposed in this study is that this methodology can be adopted across all cancer spectrums as opposed to modifications targeting certain cancer-specific markers. Importantly, administration of chemotherapeutic drug formulations at an optimal osmotic pressure and viscosity (1897 kPa, 11.5 mPa·s) through the LDDS not only enhanced the therapeutic response and minimized side effects, but also reduced the financial burden by decreasing the dosage required and increasing patient compliance by making multiple administrations to achieve sustained drug concentrations redundant. Thus, this formulation is of great translational utility and can be used as a suitable drug-delivery vehicle to enhance the therapeutic response and minimize systemic toxicity.

AUTHOR CONTRIBUTIONS

Radhika Mishra: Investigation, data curation, formal analysis, visualization, writing—original draft preparation. Ariunbuyan Sukhbaatar: Data curation, visualization, funding acquisition. Arunkumar Dorai: Resources, writing—review and editing. Shiro Mori: Validation, formal analysis. Testuya Kodama: Conceptualization, methodology, validation, project administration, writing—review and editing, supervision, funding acquisition.

ACKNOWLEDGMENTS

The study was supported by JSPS KAKENHI grant numbers 20K20161 (Ariunbuyan Sukhbaatar), 22K18203 (Ariunbuyan Sukhbaatar), 20H00655 (Tetsuya Kodama), and 21K18319 (Tetsuya Kodama), and the Suzuken Memorial Foundation (Ariunbuyan Sukhbaatar).

FUNDING INFORMATION

This work was supported by the Suzuken Memorial Foundation and the Japan Society for the Promotion of Science (20H00655, 20K20161, 21K18319, 22K18203).

DISLOSURE

No conflicts of interest.

ETHICS APPROVAL

Approval of the research protocol by an Institutional Reviewer Board: Approval obtained from the Institutional Animal Care and Use Committee of Tohoku University (2019医工動-009-04).

ANIMAL STUDIES

Guidelines of the Institutional Animal Care and Use Committee of Tohoku University which conform to the provisions of the Declarations of Helsinki were complied with for all investigations carried out using murine models.

ORCID

Ariunbuyan Sukhbaatar https://orcid.org/0000-0001-9137-2966
Tetsuya Kodama https://orcid.org/0000-0003-4727-9558

REFERENCES

1. Tateda M, Shiga K, Yoshida H, et al. Management of the patients with hypopharyngeal cancer: eight-year experience of Miyagi Cancer Center in Japan. *Tohoku J Exp Med*. 2005;205(1):65-77.
2. Shiga K, Ogawa T, Kobayashi T, et al. Malignant melanoma of the head and neck: a multi-institutional retrospective analysis of cases in northern Japan. *Head Neck*. 2012;34(11):1537-1541.
3. Chaffer CL, Weinberg RA. A perspective on cancer cell metastasis. *Science*. 2011;331(6024):1559-1564.
4. Hanahan D, Weinberg RA. Hallmarks of cancer: the next generation. *Cell*. 2011;144(5):646-674.
5. Chambers AF, Groom AC, MacDonald IC. Dissemination and growth of cancer cells in metastatic sites. *Nat Rev Cancer*. 2002;2(8):563-572.
6. Brown M, Assen FP, Leithner A, et al. Lymph node blood vessels provide exit routes for metastatic tumor cell dissemination in mice. *Science*. 2018;359(6382):1408-1411.

7. Shao LA, Takeda K, Kato S, Mori S, Kodama T. Communication between lymphatic and venous systems in mice. *J Immunol Methods*. 2015;424:100-105.
8. Pereira ER, Kedrin D, Seano G, et al. Lymph node metastases can invade local blood vessels, exit the node, and colonize distant organs in mice. *Science*. 2018;359(6382):1403-1407.
9. Punglia RS, Morrow M, Winer EP, Harris JR. Local therapy and survival in breast cancer. *N Engl J Med*. 2007;356(23):2399-2405.
10. Shao L, Ouchi T, Sakamoto M, Mori S, Kodama T. Activation of latent metastases in the lung after resection of a metastatic lymph node in a lymph node metastasis mouse model. *Biochem Biophys Res Commun*. 2015;460(3):543-548.
11. Sukhbaatar A, Mori S, Saiki Y, Takahashi T, Horii A, Kodama T. Lymph node resection induces the activation of tumor cells in the lungs. *Cancer Sci*. 2019;110(2):509-518.
12. Sukhbaatar A, Sakamoto M, Mori S, Kodama T. Analysis of tumor vascularization in a mouse model of metastatic lung cancer. *Sci Rep*. 2019;9:16029.
13. Abe H, Schmidt RA, Kulkarni K, Sennett CA, Mueller JS, Newstead GM. Axillary lymph nodes suspicious for breast cancer metastasis: sampling with US-guided 14-gauge core-needle biopsy–clinical experience in 100 patients. *Radiology*. 2009;250(1):41-49.
14. Mikada M, Sukhbaatar A, Miura Y, et al. Evaluation of the enhanced permeability and retention effect in the early stages of lymph node metastasis. *Cancer Sci*. 2017;108(5):846-852.
15. Yamaki T, Sukhbaatar A, Mishra R, et al. Characterizing perfusion defects in metastatic lymph nodes at an early stage using high-frequency ultrasound and micro-CT imaging. *Clin Exp Metastasis*. 2021;38(6):539-549.
16. Tada A, Horie S, Mori S, Kodama T. Therapeutic effect of cisplatin given with a lymphatic drug delivery system on false-negative metastatic lymph nodes. *Cancer Sci*. 2017;108(11):2115-2121.
17. Kodama T, Hatakeyama Y, Kato S, Mori S. Visualization of fluid drainage pathways in lymphatic vessels and lymph nodes using a mouse model to test a lymphatic drug delivery system. *Biomed Opt Express*. 2015;6(1):124-134.
18. Fujii H, Horie S, Sukhbaatar A, et al. Treatment of false-negative metastatic lymph nodes by a lymphatic drug delivery system with 5-fluorouracil. *Cancer Med*. 2019;8(5):2241-2251.
19. Fukumura R, Sukhbaatar A, Mishra R, Sakamoto M, Mori S, Kodama T. Study of the physicochemical properties of drugs suitable for administration using a lymphatic drug delivery system. *Cancer Sci*. 2021;112(5):1735-1745.
20. Sukhbaatar A, Mori S, Kodama T. Intranodal delivery of modified docetaxel: innovative therapeutic method to inhibit tumor cell growth in lymph nodes. *Cancer Sci*. 2022;113(4):1125-1139.
21. Yu ML, Williams M, Dixon K, et al. Intratumoral injection of gels containing losartan microspheres and (PLG-g-mPEG)-cisplatin nanoparticles improves drug penetration, retention and anti-tumor activity. *Cancer Lett*. 2019;442:396-408.
22. Munoz NM et al. Influence of injection technique, drug formulation and tumor microenvironment on intratumoral immunotherapy delivery and efficacy. *J Immunother Cancer*. 2021;9(2):e001800.
23. Kato S, Takeda K, Sukhbaatar A, et al. Intranodal pressure of a metastatic lymph node reflects the response to lymphatic drug delivery system. *Cancer Sci*. 2020;111(11):4232-4241.
24. Jain RK, Martin JD, Stylianopoulos T. The role of mechanical forces in tumor growth and therapy. *Annu Rev Biomed Eng*. 2014;16(16):321-346.
25. Jain RK, Baxter LT. Mechanisms of heterogeneous distribution of monoclonal antibodies and other macromolecules in tumors: significance of elevated interstitial pressure. *Cancer Res*. 1988;48(24 Pt 1):7022-7032.
26. Rother J, Nöding H, Mey I, Janshoff A. Atomic force microscopy-based microrheology reveals significant differences in the viscoelastic response between malign and benign cell lines. *Open Biol*. 2014;4(5):140046.
27. Yin J, Kong X, Lin W. Noninvasive cancer diagnosis in vivo based on a viscosity-activated near-infrared fluorescent probe. *Anal Chem*. 2021;93(4):2072-2081.
28. Emon B, Bauer J, Jain Y, Jung B, Saif T. Biophysics of tumor microenvironment and cancer metastasis – a mini review. *Comput Struct Biotechnol J*. 2018;16:279-287.
29. van Oosten ASG, Chen X, Chin LK, et al. Emergence of tissue-like mechanics from fibrous networks confined by close-packed cells. *Nature*. 2019;573(7772):96-101.
30. Nia HDT, Munn LL, Jain RK. CANCER physical traits of cancer. *Science*. 2020;370(6516):eaaz0868.
31. Song JW, Munn LL. Fluid forces control endothelial sprouting. *Proc Natl Acad Sci USA*. 2011;108(37):15342-15347.
32. Jain RK. Normalizing the tumor microenvironment to treat cancer: bench to bedside to biomarkers. *J Clin Oncol*. 2013;31(17):2205-2218.
33. Shao L, Mori S, Yagishita Y, et al. Lymphatic mapping of mice with systemic lymphoproliferative disorder: usefulness as an inter-lymph node metastasis model of cancer. *J Immunol Methods*. 2013;389(1–2):69-78.
34. Song WT, Tang Z, Zhang D, Burton N, Driessenb W, Chen X. Comprehensive studies of pharmacokinetics and biodistribution of indocyanine green and liposomal indocyanine green by multispectral optoacoustic tomography. *RSC Adv*. 2015;5(5):3807-3813.
35. Iwamura R, Sakamoto M, Mori S, Kodama T. Imaging of the mouse lymphatic sinus during early stage lymph node metastasis using intranodal lymphangiography with X-ray micro-computed tomography. *Mol Imaging Biol*. 2019;21(5):825-834.
36. Falandry C, Rousseau F, Mouret-Reynier MA. Efficacy and safety of first-line single-agent carboplatin vs carboplatin plus paclitaxel for vulnerable older adult women with ovarian cancer: a GINECO/GCIG randomized clinical trial. *JAMA Oncol*. 2021;7(6):853-861.

SUPPORTING INFORMATION

Additional supporting information can be found online in the Supporting Information section at the end of this article.

How to cite this article: Mishra R, Sukhbaatar A, Dorai A, Mori S, Shiga K, Kodama T. Drug formulation augments the therapeutic response of carboplatin administered through a lymphatic drug delivery system. *Cancer Sci*. 2023;114:259-270. doi: 10.1111/cas.15599